
A novel experimental approach to quantitatively evaluate the printability of inks in 3D printing using two criteria

Haohao Ji ^{a,b}, Jin Zhao ^a, Jie Chen ^c, Shunzo Shimai ^a, Jian Zhang ^{a,b,*}, Yu Liu ^{c,*},
Dianzi Liu ^{d,*}, Shiwei Wang ^{a,b}

^a State Key Laboratory of High Performance Ceramics and Superfine Microstructure, Shanghai Institute of Ceramics, Chinese Academy of Sciences, Shanghai 200050, China

^b Center of Materials Science and Optoelectronics Engineering, University of Chinese Academy of Sciences, Beijing 100049, China

^c School of Mechanical Engineering, Jiangnan University, Wuxi, Jiangsu 214122, China

^d School of Engineering, University of East Anglia, Norwich NR4 7TJ, UK

* Corresponding authors.

E-mail address: jianzhang@mail.sic.ac.cn (J. Zhang),

yuliu@jiangnan.edu.cn (Y. Liu),

Dianzi.Liu@uea.ac.uk (D. Z. Liu).

Abstract

Material extrusion enables deposition of filaments with designed structures, and such sub-categories as direct ink writing brings increasing possibilities for the fabrication of multi-material and complex-shaped high-performance fully dense components. It has been well understood that the critical requirement for successful direct ink writing is the printability of inks. To address this challenge arising from direct ink writing, a novel experimental approach that takes advantages of the developed rotational rheology test and capillary rheology test, has been proposed to evaluate the printability of inks. The inks used for evaluation have been

prepared from the water-based slurries of Al_2O_3 , Y_2O_3 and Nd_2O_3 ceramic powders according to the stoichiometry ratio of $\text{Y}_3\text{Al}_5\text{O}_{12}/\text{Y}_{2.982}\text{Nd}_{0.018}\text{Al}_5\text{O}_{12}$ with the different addition of hydroxyethyl cellulose. The parameters setting in rotational rheology test including the low strain value within the linear viscoelastic region (0.4%) and the high shear rate (85 s^{-1}) of the inks have been determined by amplitude sweep test and theoretical analysis and calculation, respectively. Two criteria - storage modulus and extrusion stress - have been first introduced to assess the success of inks applicable in direct ink writing. Using these criteria, the excellent qualities of printable inks have been quantitatively defined with the values in the range of 2300-6000 Pa and 401-430 Pa, respectively. Moreover, the significant influence of pre-pressure on the uniform extrusion of inks has been analysed in capillary extrusion experiments and results have provided a useful insight into the technology development of suppressing the appearance of bubbles. The flow velocity distribution of inks along the nozzle diameter has been compared based on the non-Newtonian index n , and the results have shown that the smaller the value n of the ink represents, the smoother the flow velocity distribution along the nozzle diameter is. Finally, the correctness of the proposed approach has been further examined by a transparent ceramic ink, which is prepared by mixing transparent ceramic powders with neodymium oxides. The prediction has agreed well with the experimental results and the in-line transmittance (84.4%) of the transparent ceramic at 1064 nm is close to the theoretical value.

Keywords: Ceramics direct ink writing; Printability; Rotational rheology; Capillary rheology.

1. Introduction

Additive manufacturing is attracting broad scientific interests for forming the complex three-dimensional objects [1, 2], which consist of layered patterns through computational slicing. Direct ink writing (DIW), one of the state-of-art 3D printing technologies, has been widely investigated owing to its compatibility with a broader range of ink materials, which has been

used to generate transparent ceramics with controllable doping profile [3, 4] for multi-scale structures [5-9]. For direct 3D writing of dense networks, as the inks which are extruded from the nozzle still possess the fluid property to some extent, they could fill the void space between filaments and maintain the shaped profile in a proper range, as shown in Fig. 1. Moreover, the flow velocity of the ink along the nozzle diameter should be distributed as uniformly as possible to avoid lamination defects during extrusion [10, 11]. To achieve this goal, the straightforward method is to adjust rheological properties of ceramic inks so that they behave shear-thinning during extrusion, but have the ability to quickly recover the storage modulus after extrusion. For transparent ceramic DIW [3, 4], in order to enhance the mechanical and optical performance of ceramic parts, there has been an increasing demand for the high solids loading ink to alleviate deformation or cracking arising from the debinding processes of the green bodies [2].

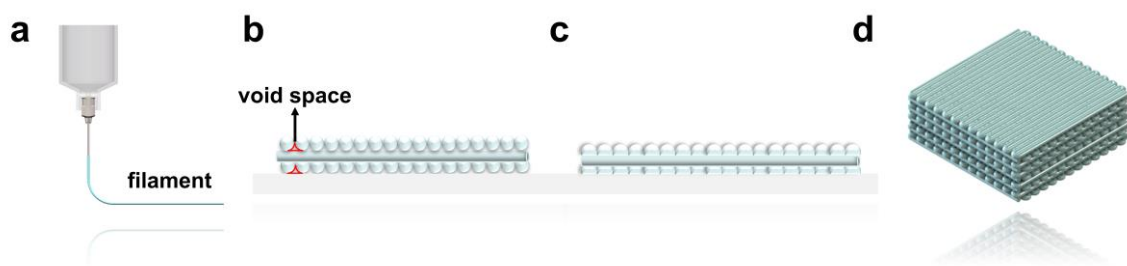


Fig. 1. Dense structure forming process. (a) Shear-thinning and Extrusion, (b) Deposition, (c) Flowing and filling void space, (d) Drying.

Research on the printability of inks for DIW has also been investigated by many scientists. Though the morphology of the ink after writing could be observed, this process is time-consuming and laborious. Also, the rheological parameters that define the printability are quite uncertain due to the fact that the measurements highly depend on the characteristics of the inks, such as solids loading, particle size and morphology, type of solvent, and nozzle motion [9, 12]. Therefore, establishing an evaluation strategy for predicting ink printability

has attracted more attention to address the aforementioned problems. Andrew et al. [12] studied the extensional and shear rheology of graphene oxide (G.O.) suspensions and focused on three rheological parameters including storage modulus, solid-liquid transition stress and the flow transition index, to predict the printability. Despite the use of multi-step oscillatory sequence to simulate the extrusion process, the severe limitation was observed that the high strain scanning cannot reflect the violent shearing effect experienced by the ink. M' Barki et al. [13] used the time characteristics of boehmite gelation to study the relationship between printability and time-dependent rheological behaviour. The mathematical model established was only valid for hydrogel inks with low solids loading.

Inspired by the traditional extrusion process, the influence of bubbles on density, the gradient pressure and the interaction with the capillary wall including wall sliding [14] and liquid phase migration [15], could be investigated for improving the understanding of the ink printability. Jae et al. [16] adopted a double-tube capillary rheometer to study the effects of the binder composition on rheological properties of lead magnesium niobate-lead zirconate titanate (PMN-PZT) ceramic feedstock at different shear rates and temperatures.

Unfortunately, the study failed to reflect the changes in rheological properties of the feedstock due to the effect of liquid phase migration. Shabnam et al. [17] combined a ram extruder with a universal mechanical testing machine to analyse the influence of initial water content, extrusion speed and die length on the extrusion pressure, but the whole process required several dies with different length-diameter ratios and a large number of experiments to obtain sufficient data. Despite the extrusion-based mechanism of DIW for producing ceramics, DIW indeed is an additive manufacturing method heavily utilized to generate structures in meso- and micro-scales [18].

In this paper, a novel experimental approach taking advantages of the integration of the developed oscillation-rotation-oscillation (O.R.O.) test (for rheological parameters) and capillary extrusion (for displacement-pressure curve) test, has been proposed to quantitatively

evaluate the printability of ceramic inks. The influence of ink structure recovery capacity and velocity distribution along the capillary diameter of the capillary on its printability has been analysed for in-depth understanding on the preparation of high-quality printable inks for DIW. Moreover, the changes in rheological characteristics of inks during extrusion have been discussed to facilitate the fabrication of green bodies without defects from direct ink writing. The developed method enabling qualitative and quantitative evaluations of the printability of aqueous ceramic particle suspensions has been successfully demonstrated by DIW of dense structures.

2. Materials and methods

2.1. Ceramic ink preparation

The ceramic powder has been obtained by mixing Al_2O_3 (99.99 wt. % purity, Taimei Chemical Co., Ltd, Japan) and Y_2O_3 (99.99 wt. % purity, Jiahua Advanced Material Resources Co., Ltd, Jiangyin, China) powder according to the stoichiometry ratio of $\text{Y}_3\text{Al}_5\text{O}_{12}$. More details have been provided by the research [19]. Then, the pre-mixed powder, deionized water and dispersant (0.6 wt. %, Dolapix CE - 64, Zschimmer & Schwarz, Germany) have been mixed and ball milled for 1 hour to obtain low viscosity inks. Next, the rheological characteristics of the inks have been further adjusted by adding hydroxyethyl cellulose (HEC, Shanghai Macklin Biochemical Co., Ltd., 3400-5000 mPa·s, China). Finally, twelve different inks have been successfully prepared by changing the contents of solids loading and the HEC contents, as shown in Table 1. The preparation of the 0.6 at. % Nd: YAG ceramic ink is similar to that of the undoped YAG ceramic ink described above. The difference is that Nd_2O_3 powder (99.99 wt. % purity, Rare-Chem. Hi-Tech. Co., Ltd, Huizhou, China) is added according to the stoichiometric ratio of $\text{Y}_{2.982}\text{Nd}_{0.018}\text{Al}_5\text{O}_{12}$ in the powder preparation process and the addition of HEC is 0.3 wt. %.

Table 1

Experiment groups.

Ink ID	G1	G2	G3	G4	G5	G6	G7	G8	G9	G10	G11	G12
Solids Loading [vol. %]		48				50				52		
HEC [wt. %]	0	0.20	0.38	0.50	0	0.20	0.38	0.50	0	0.20	0.30	0.38

2.2. O.R.O. test

The structural recovery capacity of the inks has been characterized by the developed O.R.O. (oscillation-rotation-oscillation) test, which is achieved by a rotational rheometer (Haake Viscotester iQ Air, Thermo Electron GmbH, Germany) at 25 °C using a 20 mm diameter flat plate with the design gap of 0.1 mm. The amplitude sweep (Control Shear Stress (C.S.S.) mode with a fixed frequency of 1 Hz, stress range of 0.005~500 Pa) has been adopted to determine the linear viscoelastic region (L.V.R.) of the ink. The printability of the ink has been classically evaluated by a three-stage thixotropy test called O.R.O. The first stage is an extremely low-shear oscillation (L.S.O.) test (Controlled Shear Deformation (C.S.D.) mode with a fixed frequency at 1 Hz, 120 s). The second stage is a high-shear rotational (H.S.R.) test (Controlled Shear Rate (C.S.R.) mode with a fixed frequency at 1 Hz and a crescent shear rate for 30 s). The third stage is again a shear oscillation test with the same parameter setting at the first stage. The non-Newtonian index of the ink is equal to the slope of the double logarithmic coordinates curve in $\ln\sigma\text{-}\ln\dot{\gamma}$, where σ is the shear stress and $\dot{\gamma}$ is the shear rate. The relationship between ink shear stress and shear rate can be obtained by rotational test (Controlled Shear Rate (C.S.R.) mode with a fixed frequency at 1 Hz and shear range between 0~500 s⁻¹).

2.3. Capillary extrusion test

The liquid phase migration degree of inks has been characterized by the capillary extrusion test. In order to simplify the process in the capillary rheology test, an extrusion mould shown in Fig. 2 has been developed. The piston is driven by the head from a universal mechanical

testing machine (Instron-5566, Instron, U.S.A.) for vertically movements at a constant speed. During the experiment, the volume flow rate of inks determines the speed of the piston during the experiment, which is $0.36 \text{ mm} \cdot \text{min}^{-1}$. The relationship between the piston pressure and displacement has been recorded by the pressure sensor of Instron-5566, and the ink extrusion process has been observed through the support structure window. It has been noted that the pressure fluctuation has the remarkably effect on the stability of ink extrusion. The printability of different inks has been initially judged through the qualitative analysis of the morphology (continuity and shape retention) during the extrusion test. Furthermore, the relationship between the extrusion stress and the printability has been quantitatively analysed.

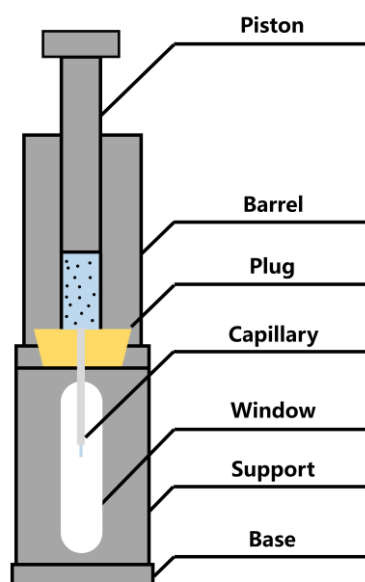


Fig. 2. Capillary extrusion mould.

2.4. Direct ink writing

Based on the aforementioned experimental tests, inks with the pre-defined storage modulus and extrusion stress quantitatively evaluated by two criteria in this paper have been selected and written by a homemade DIW printer, which is a computer-controlled 3-axis gantry platform for the generation of structures made of printable materials. The inks are initially

pushed by air pressure through a syringe nozzle with an inner diameter of 0.61 mm, and then they are deposited on a glass plate coated with Teflon. The layer height is 0.4 mm, the line spacing is 0.72 mm and the printing speed is 4 mm/s. For the ink prepared from doped Nd_2O_3 powder, the layer height is 0.3 mm, the line spacing is 0.6 mm and the printing speed is 4 mm/s. Printing paths are compiled as parameterized G-code scripts, and all movements are programmed in LabView. The samples are filled with grid-like filaments. The printing path of each layer is a single zig-zag trace and the line directions of odd-numbered and even-numbered layers are perpendicular to each other ((See Fig. S1 in supporting information).

3. Results and discussion

During the extrusion process, the ink has experienced three main phases including: (1) static, (2) high-speed shear, and (3) static state successively. To evaluate the structure recovery capacity of the ink, a three-stage thixotropy test of oscillation-rotation-oscillation, called O.R.O., has been developed to reflect the change process in rheological properties of inks during extrusion, as shown in Fig. 3. In the first stage, an extremely low-shear oscillation (L.S.O.) test has been conducted to simulate the static state of the ink in the syringe. It is noted that a low strain value within the linear viscoelastic region, where the stress at this strain value is less than the yield point τ_y , should be applied in this phase. Following this, a high-shear rotational (H.S.R.) test with a shear rate close to that occurs when the ink is extruded from the nozzle, has been performed to simulate the change in viscosity in the second stage. The reason for the rotation test instead of the oscillation test in this stage lies in the fact that it is extremely difficult to accurately reflect the shear experience of the ink during extrusion, even a high strain amplitude is applied in the oscillation test [20]. Finally, a shear oscillation test used in the first stage has been carried out again to represent the structure recovery of the ink after extrusion. It has been observed that the parameter setting in the O.R.O. test including the low strain value within the linear viscoelastic region and the high shear rate, is crucial to precisely evaluate the printability of the ink discussed in details in the

following sections.

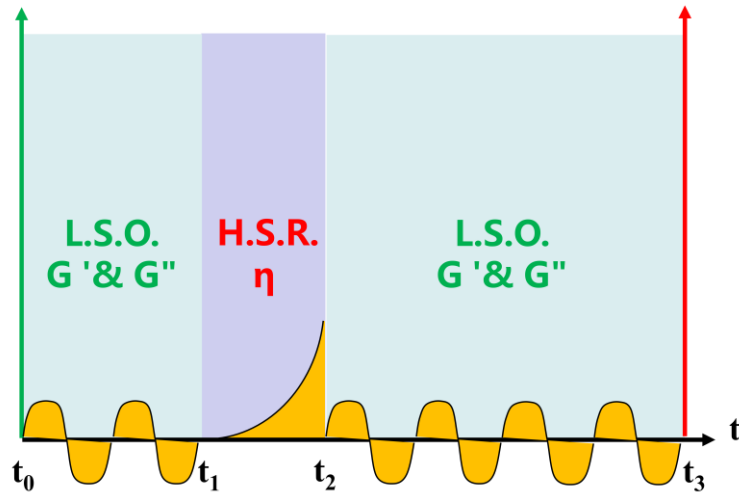


Fig. 3. Schematic diagram of the developed O.R.O mode test.

3.1. Measurement of low strain value within linear viscoelastic region

In the amplitude sweep test, the low strain value of the inks can be measured to represent the physical behaviour within the linear viscoelastic region. Furthermore, the amplitude sweep curves have the potential to reflect the solid-liquid transition characteristics of different inks, which is considered a criterion to evaluate the ink printability. In Fig. 4, amplitude sweep curves of the inks with and without HEC addition have been compared to demonstrate that the ink with solid-liquid transition characteristics should have a yield point and a flow point. It can be observed that the inks with adding HEC exhibit better performances including the distinct representations of the yield point τ_y that is represented by the linear viscoelastic boundary, and the flow point τ_f , which is determined by the equation of G' (storage modulus) = G'' (loss modulus).

In Fig. 4a-c, there is no clear intersection point for the curves, which represent the relationships for shear stress, G' and G'' . While, two distinct curves intersected at the flow point τ_f can be observed in Fig. 4d-f. This remarkable transition process from the solid-like

behaviour to the liquid-like behaviour owes to the addition of HEC in the ink. Furthermore, if the stress applied is less than τ_y , the ink mainly exhibits the solid-like behaviour. Otherwise, the more liquid-like behaviour possessed by the ink will be demonstrated. In the zone bounded by the yield point and the flow point, a transitional state that displays gradual softening has been identified.

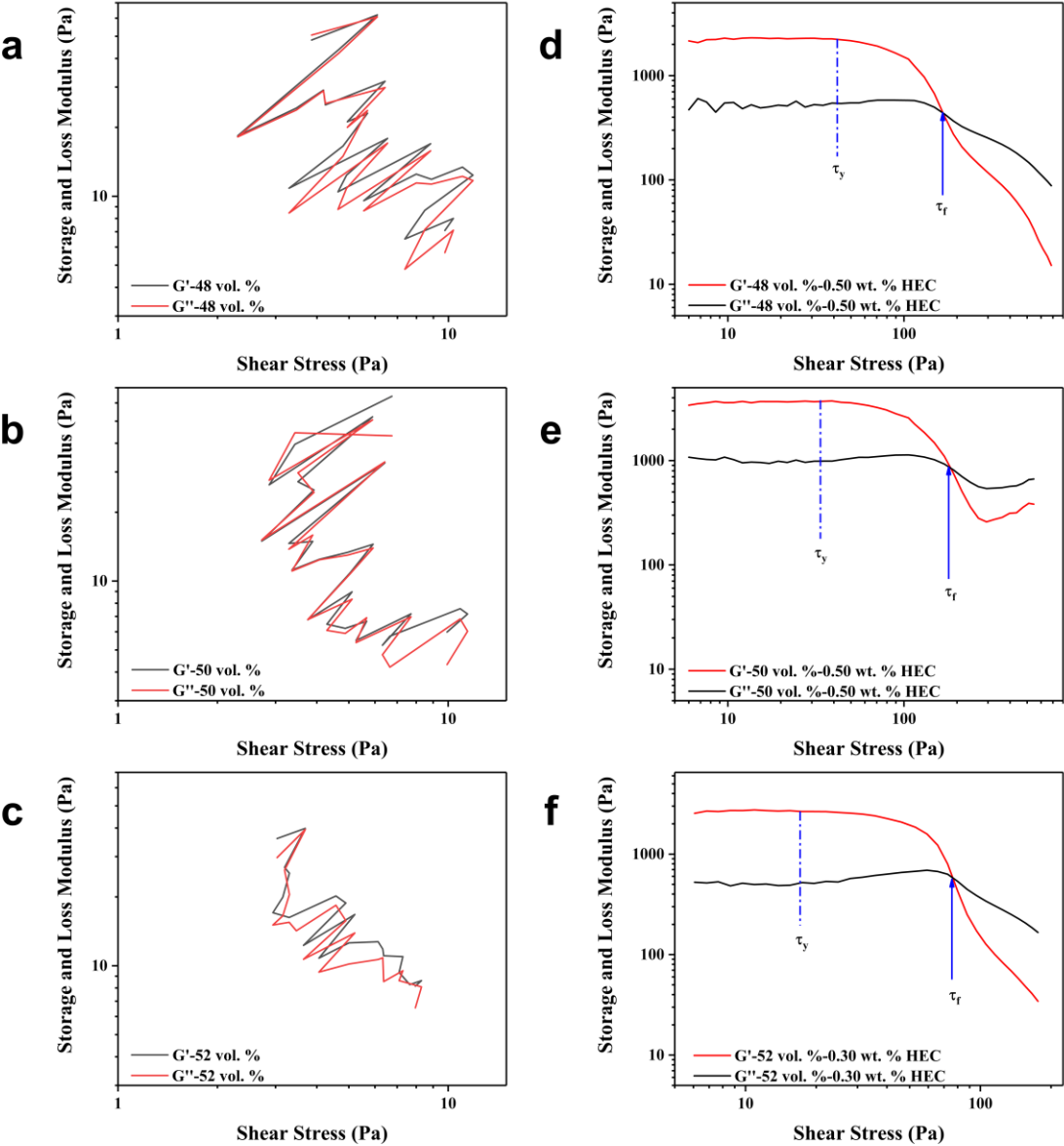


Fig. 4. Amplitude sweep curves of inks with different solids loading. (a-c) without HEC, (d-f)

with HEC.

Fig. 5a-c has described the effects of HEC on the amplitude sweep curves of inks. With the different values of solids loading, both the yield point and the flow point increase as HEC addition increases. For example, the yield point and the flow point of the ink with 50 vol. % solids loading increase from 20 Pa and 57 Pa to 38 Pa and 175 Pa when HEC is increased from 0.20 wt. % to 0.50 wt. %, respectively. It is worth noting that adding HEC has significantly enhanced the plasticity of inks. In Fig. 5d, the disruptive influence of the solids loading on the yield point and flow point can be observed. The storage and loss moduli of the ink with 0.38 wt. % HEC have been remarkably increased as a slight increase of yield point. Similarly, the same conclusion on the flow point can also be drawn, which indicates the control of liquid-like behaviour of inks is extremely difficult. This has been demonstrated by the results representing the continuous change of the yield point value (A-B-C) and flow point value (D-E-F) in Figure 4a-c and the abrupt variation in Fig. 5d.

Actually, the flow point of inks with good printability, to some extent, is able to represent a suitable pressure for extrusion. As a result, the printing resolution has been maintained during the deposition and the flow has been easily induced to fill the gap. The lower flow point means that the ink can be squeezed out under the lower pressure, however this will lead to the structural deformation due to the gravity after extrusion. Moreover, it is challenging to stabilize the extrusion rate when the lower pressure is applied, and its fluctuation has a significant impact on the morphological control during printing.

In contrast, a high flow point means that the ink needs higher pressure to be squeezed out. During the process of squeezing out inks, the liquid phase has remarkable effects on the particles surrounding, the separation from each other and the promotion of their mutual sliding. The capillary force generated by the liquid bridge among particles in the deflocculation system is considered the main component of the cohesive force that keeps the

particles in a uniform plastic substance [21]. Since the ceramic particles are lubricated by water and moved under pressure, the excessive pressure may cause the liquid to be drained out of the ink quickly, known as liquid phase migration [22, 23]. This commonly occurs as the water stored in the micro pores among the particles more easily moves than the particles due to the frictions from their interactions and the abrasion originated from the syringe wall. Then, the pressure is transmitted to the ceramic particles. This usually results in the uneven distribution of the water in the pressure direction and affects the stability of the flow rate and the uniformity of the green bodies. Furthermore, there has been no effective solutions to the equipment design and the performance control of the green bodies for the force exerted and force release on the ceramic particles.

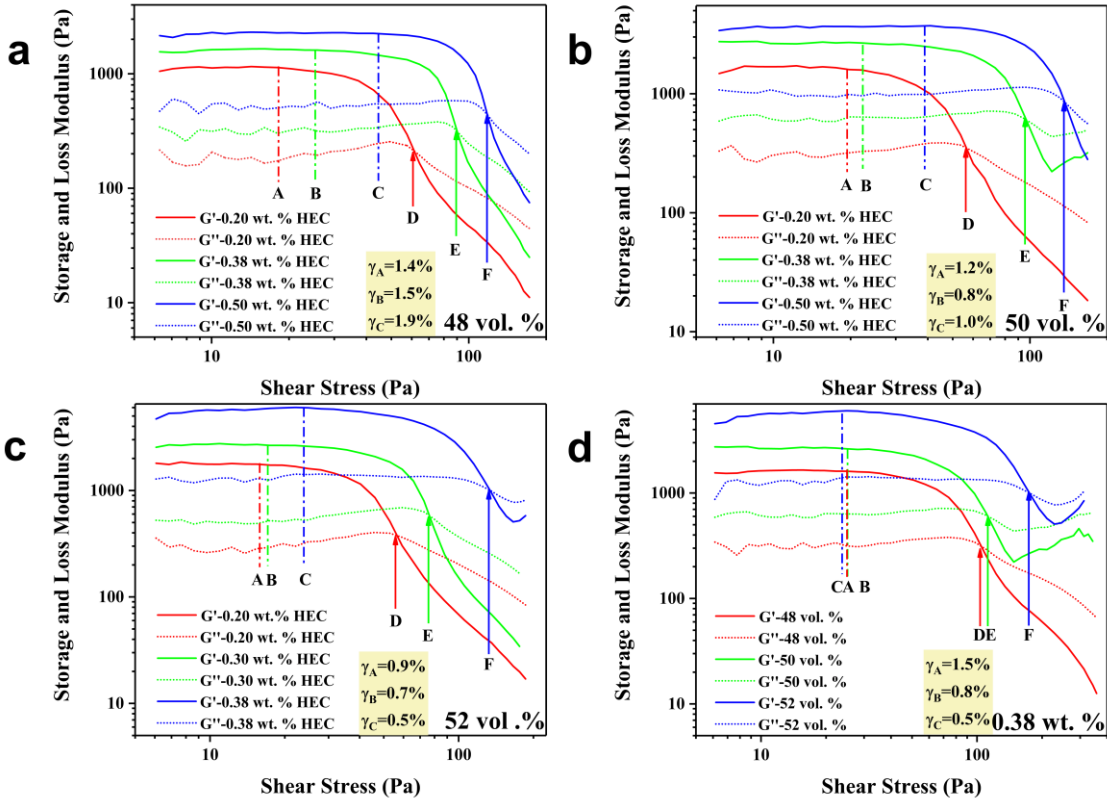


Fig. 5. Amplitude sweep curves of inks with different HEC addition. (a) 48 vol. %, (b) 50 vol. %, (c) 52 vol. % and (d) 0.38 wt. % HEC with different solids loading. γ represents the strain value of different inks at the linear viscoelastic boundary.

Normally, printable inks will flow only when a certain pressure is applied, and this can be described as a transition process from the solid-like behaviour to the liquid-like behaviour. Therefore, the basic condition required by the printable ink is the existence of a specific flow point, which indicates that the inks of G1, G5 and G9 (Table 1) cannot be used for printing. Therefore, experimental tests and evaluations should be carried out to define the range of the flow point of inks for the good printability. Based on the results in Fig. 5, the strain (0.4%) has been selected as the threshold value to reflect the solid-like behaviour under the static state in the oscillation stage of O.R.O. test.

3.2. Theoretical analysis and calculation of high shear rate

To reflect the changes in the rheological properties of inks during the actual extrusion process in the proposed O.R.O. test, the shear rate in the rotation stage should be determined. The shear stress distribution along the diameter can be formulated by Eq. (1) [24, 25]:

$$\tau = \sigma_{rz} = \frac{\partial p}{\partial z} \cdot \frac{r}{2} \quad (1a)$$

$$\sigma_{rz}|_{r=0} = 0 \quad (1b)$$

$$\sigma_{rz}|_{r=R} = \frac{\partial p}{\partial z} \cdot \frac{R}{2} \quad (1c)$$

where τ denotes the shear stress, $\frac{\partial p}{\partial z}$ represents the axial pressure gradient, r is the distance from the axis, and R is the radius of the capillary. It can be observed that the shear stress distribution over the cross-section of the capillary is not uniform, but proportional to the distance r . The shear rate at the centre of the cross-sections is zero, and its maximum value occurs at the outer diameter of the tube. Therefore, the shear rate value at the capillary wall has been chosen as the input for the rotation stage of O.R.O. test. The apparent shear rate of Newtonian fluid on the capillary wall ($\dot{\gamma}_w$) can be determined by Eq. (2) [26]:

$$\dot{\gamma}_w = \frac{4Q}{\pi R^3} = \frac{8}{D} v_z \quad (2)$$

where Q represents the volume flow rate of the ink, D is the capillary diameter, v_z is the average flow rate of the ink. In practice, v_z and D are given by the printing requirements. Therefore, the value of 52 s^{-1} for the apparent shear rate $\dot{\gamma}_w$ has been used in this study. As the general ceramic slurry belongs to a non-Newtonian fluid, the true shear rate is different from the result calculated by Eq. (2). Therefore, the shear rate ($\dot{\gamma}$) of non-Newtonian fluid flowing through the capillary wall can be accurately calculated by Eq. (3) [27, 28]:

$$\dot{\gamma} = \frac{\dot{\gamma}_w}{4} \left(\frac{d \ln \dot{\gamma}_w}{d \ln \sigma_{rz}} + 3 \right) \quad (3)$$

where $\dot{\gamma}_w$ is the apparent shear rate calculated by Eq. (2). The non-Newtonian index of the ink used in this study is about 0.3, which can be obtained from the curve fitting of data from a simple viscosity test with a pseudoplastic fluid power law function. Thus, the true shear rate of 85 s^{-1} in the rotation stage of O.R.O. test has been adopted.

3.3. Structural recovery capability of inks

The structural recovery capability of the ink, which is the most important criterion to evaluate the ink printability, reflects the extent to which the filament structure and profile are maintained after a strong shear action. As the low strain and high shear rate have been determined throughout the amplitude sweep test and theoretical analysis in Section 3.1 and Section 3.2, the proposed O.R.O. test can be conducted to characterize the structure recovery capability of the ink, as shown in Fig. 6. It can be observed that the curves representing the variations of storage and loss moduli for the inks without HEC (Fig. 6a-c) intersect several times and therefore the solid-like behaviour of such inks subject to the static condition is hardly exhibited. While, inks with HEC addition have possessed such property, which is indicated by both a lower viscosity during extrusion and the recovery of the solid

characteristics after extrusion. These conclusions have well agreed with the amplitude sweep results. Compared with the reported multi-step oscillation test [12], the developed O.R.O. test exhibits the following two advantages. On the one hand, the low strain value conducted to simulate the static state of the ink in this work has been determined by measuring the linear viscoelastic region obtained from amplitude sweep test, rather than arbitrarily setting a low value. On the other hand, a rotational test has been performed to simulate the change in viscosity in the second stage. Moreover, the high shear rate in the rotation stage has been determined through theoretical analysis and calculation, which means that the test parameters in this stage can be flexibly adjusted according to the process parameters during printing, so that it can be more effectively used to evaluate the printability of the ink. Andrew and colleagues [12] used a fixed strain value to simulate the structural evolution of the ink during extrusion. Obviously, it is unreasonable to use the same strain value for different materials and different process parameters, because it is extremely difficult to accurately reflect the shear experience of the ink during extrusion, even a high strain amplitude is applied in the oscillation test. For example, boehmite suspensions prepared by M' Barki and colleagues [13] exhibited solid-like behaviour even at the strain approaching 10%.

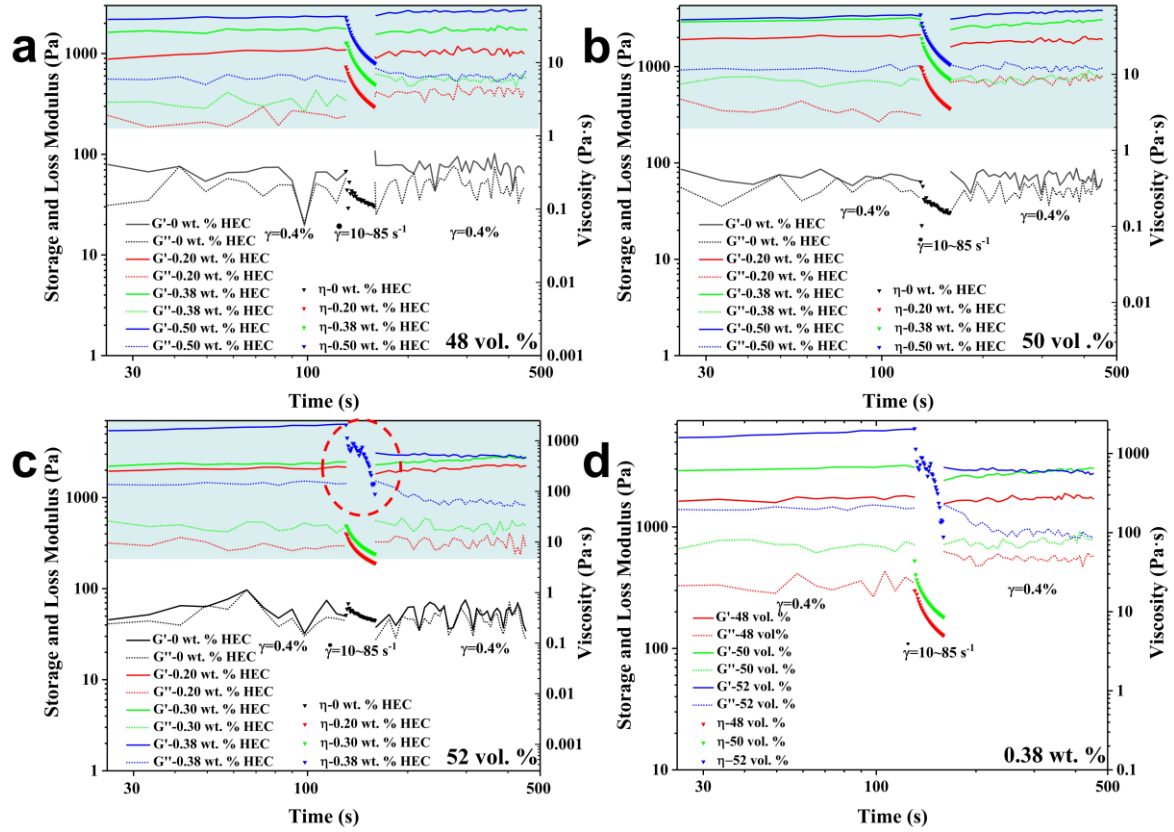


Fig. 6. O.R.O. curves of inks with different HEC addition. (a) 48 vol. %, (b) 50 vol. %, (c) 52 vol. % and (d) 0.38 wt. % HEC with different solids loading.

For inks prepared from different solids loading slurries, the storage modulus under the static condition increases as the HEC content increases in Fig. 6a-c. Also, the solids loading could influence the storage modulus proportionally shown in Fig. 6d. Most of the inks have exhibited the shear thinning behaviour and could quickly recover the original storage modulus after a strong shear action. For the ink with the solids loading of 52 vol. % and the HEC addition of 0.38 wt. %, the shear thickening occurs, where is marked by the dashed line in Fig. 6c so that it cannot be evenly and continuously squeezed out and the structure could not effectively recover after shearing. The thickening mechanism of the ink lies in cellulose swelling due to the absorption of free water in the crystalline and amorphous regions [29]. According to the requirements of DIW, the printable inks should exhibit shear thinning

behaviour in the second stage of the O.R.O. test. Once the shear action is removed, the deformation of inks will disappear due to the static storage modulus. Therefore, inks without the characteristics including the structural recovery (G1, G5 and G9) and the shear thinning during extrusion (G12) shown in Table 1 are not suitable for DIW printing. Furthermore, the ink printability also depends on the magnitude of storage modulus under static conditions, which will be discussed in the following sections.

3.4. Liquid phase migration degree of inks

As the rheological properties of the ink cannot be well understood just by the rotational rheometer test due to the facts that the results have no ability to reflect the continuity of the ink during the extrusion process and some influencing factors such as liquid phase migration exist, a self-made mould and a universal mechanical testing machine have been integrated to simulate the ink extrusion process so that the influence of the pressure and the interaction between ink and the tube wall on the rheological properties of inks in DIW can be investigated with details. If the liquid phase migration exists, the flow rate of the ink will decrease. This will lead to both structural deformations under a constant pressure condition and the uneven density of green bodies.

Based on the morphology after extrusion, the ink continuity and shape retention can be observed in Fig. 7. As the HEC content increases, the length that the ink can maintain after extrusion increases. This closely relates to the continuity and shape retention. The chain structure formed by HEC increases the consistency of the inks so that they are not easily cracked during extrusion. Since the inks of G1, G5, and G9 in Table 1 form droplets after extrusion, they cannot be used for printing due to the lack of shape retention. Though the ink lengths of G2, G3, G6 and G10 are longer, they still tend to form large droplets and could not maintain the shape of the nozzle. It has been noted that the inks of G4, G7, G8 and G11 have shown the good continuity and shape retention, except for the increase in radius due to the

extrusion swelling. Surprisingly, it has been observed that some continuous filaments appear when the ink of G12 is extruded. This could result from the high HEC content. In conclusion, inks with the good printability (for example G4, G7, G8 and G11 in Table 1) have been preliminarily defined using the morphology after extrusion.

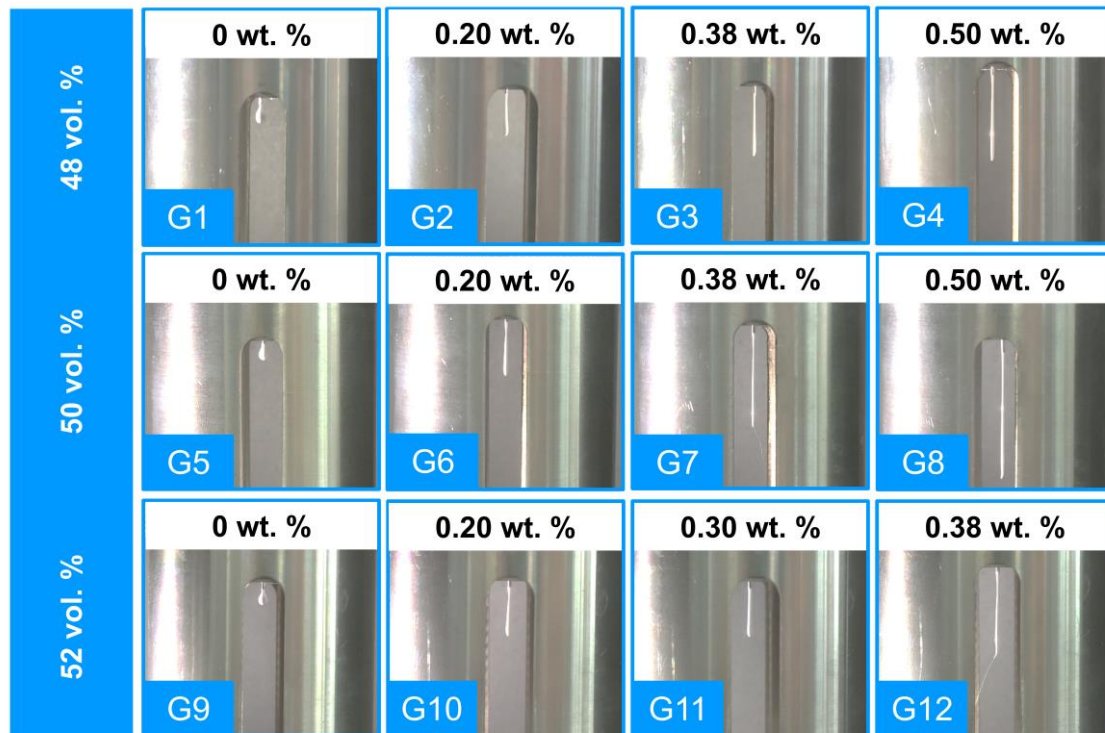


Fig. 7. The morphology of different inks when extruded.

In order to study the changes in rheological characteristics of the ink during the extrusion process, the displacement-pressure curves have been given in Fig. 8 by the analysis of data from the sensor. As compared with the curves for non-printable inks without HEC, a clear peak can be observed for printable inks with HEC. This feature indicates that making the ink flow can be achieved by applying a pressure higher than that corresponding to the peak force, which agrees well with the flow point obtained in the rotational rheology test. For inks with different solids loading, the required extrusion pressure increases as the HEC content increases. This observation is consistent with the result from the rotational rheometer test,

where the flow point increases when the increase of HEC content occurs.

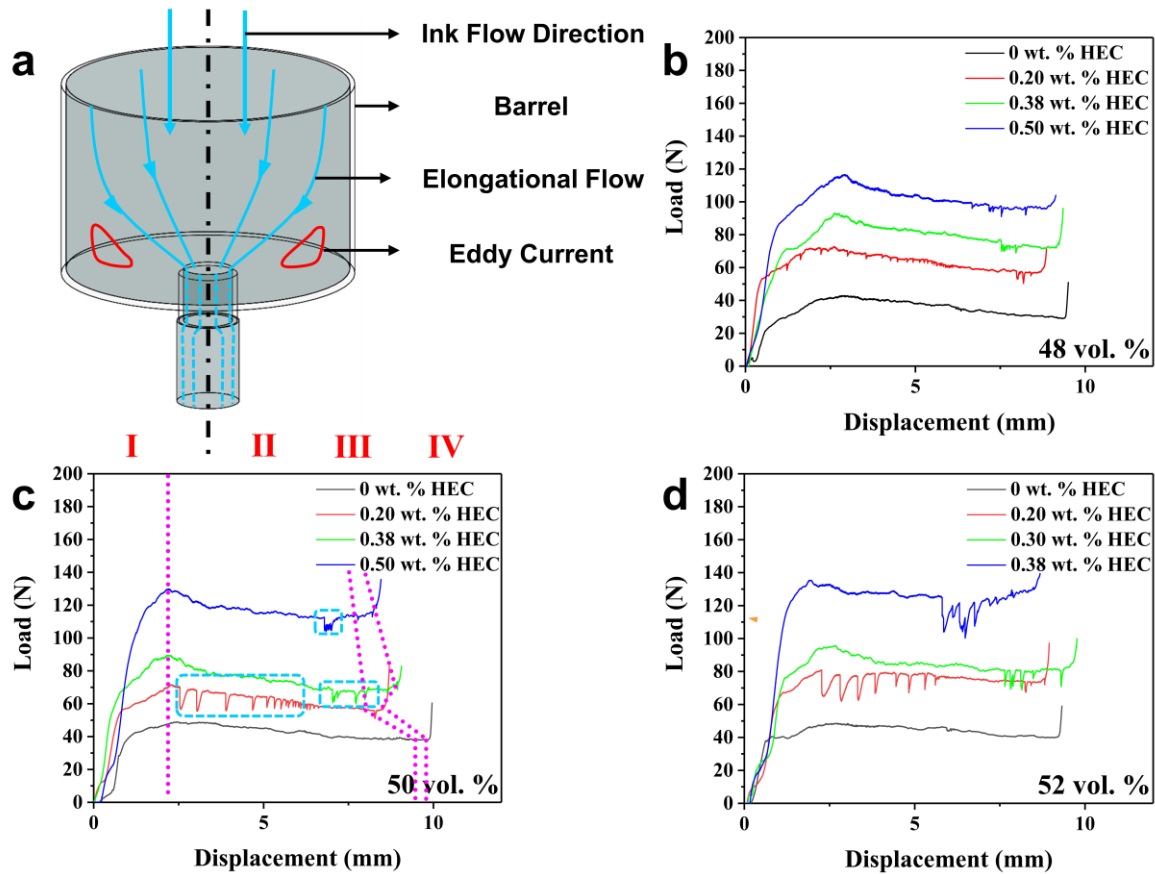


Fig. 8. (a) Schematic diagram of the distribution of streamlines in the barrel and capillary. Capillary extrusion pressure curves of inks. (b) 48 vol. %, (c) 50 vol. % and (d) 52 vol. % with different HEC addition.

Taking the ink with 50 vol. % solids loading as an example shown in Fig. 8c, the changes in the rheological characteristics during extrusion and their influence on the printability have been discussed as follows. According to the characteristics of pressure changes, the extrusion curves have been divided into four zones below:

Zone (I): The most obvious feature in this region is the linear increase of pressure with the

displacement. As the work done by the external force is converted into elastic deformation energy, the volume contraction of the ink proportional to the pressure can be observed in this zone. Also, the ink will not flow until the pressure reaches the peak value.

Zone (II): In this region, the pressure tends to be constant and decreases slowly. The rapid drop after the maximum pressure value owes to the fact that the friction of mould reduces due to the wetting by the moving ink. The subsequent decrease indicates that the water in the ink does not move along the pressure direction. This means that there is no liquid phase migration [30]. With the sudden drop of pressure shown in the blue box of Fig. 8c, bubbles are observed at the end of capillary. For the ink with the HEC addition of 0.20 wt. % in Fig. 8b-d, the drop point of the pressure appears just after the ink begins to flow. The reason behind lies in that the low viscosity of the ink makes bubbles easy to move, and then the micro bubbles gradually grow into large bubbles squeezed out. For inks without HEC, the viscosity is quite lower and there are barely bubbles after degassing. For inks with HEC, bubbles are difficult to move in the ink and tend to appear in the second half of extrusion as the continuous shearing leads to the decrease in viscosity of the ink. This can be explained by the analysis of the volume flow rate through the capillary formulated by Eq. (4) [24]:

$$Q = \int_0^R v_z \cdot 2\pi r dr = \int_0^R \frac{\pi}{2\eta_0} \frac{\partial p}{\partial z} r (R^2 - r^2) dr = \frac{\pi R^4}{8\eta_0} \cdot \frac{\partial p}{\partial z} \quad (4)$$

When the flow rate is constant, the pressure required for extrusion decreases as the viscosity of the ink decreases.

Zone (III): It can be observed that the pressure increases rapidly along with the increase of the displacement in this region. As shown in Fig. 8a, the eddy current of the ink is slow and difficult to flow due to the sharp corner, which usually results in a sharp rise in pressure toward the end of the process.

Zone (IV): In this region, the piston reaches the limit point of the displacement as the pressure increases linearly. To conclude the whole process of extrusion, three phases should be noted as follows: First, before the ink is added to the barrel, it must be fully degassed for the removal of all bubbles. Then, a simple degassing is further conducted to remove the large bubbles introduced during the addition. Second, the ink should be continuously extruded out from nozzle by the pressure in advance before the ink is used for writing. In this way, the energy absorbed by the ink can be converted into elastic energy. Once the pressure applied exceeds the value at the flow point, the ink has the ability to quickly flow and extrude out. Finally, the usage of the ink left at the end of the syringe should be avoided because the ink with good printability has the high viscosity, and thus there should be more bubbles in the remaining inks. Summarily, the conclusions drawn from the extrusion pressure curves are instructive and provide researchers a useful insight into the understanding of rheological characteristics for the fabrication of green bodies without defects from direct ink writing.

3.5. Flow velocity distribution of inks

The printability of the ink can also be evaluated by the flow velocity distribution along the nozzle diameter, which is closely related to the non-Newtonian index n [10]. To obtain the index n , the curve fitting of experimental data using Eq. (5), which describes the slope of the curve in the double logarithmic coordinates of $\ln\sigma$ - $\ln\dot{\gamma}$, has been conducted.

$$n = \frac{d(\ln\sigma)}{d(\ln\dot{\gamma})} \quad (5)$$

The velocity distribution of the fluid in the capillary can be determined by Eq. (6) [24]:

$$v_z(r) = \langle v_z \rangle \left(\frac{3n+1}{n+1} \right) \left[1 - \left(\frac{r}{R} \right)^{\frac{n+1}{n}} \right] \quad (6)$$

Figs. 9a and 9b are the n -value fitting curves of different solids loading inks without HEC and

with HEC, respectively. It can be observed that the n of the inks drops drastically after adding HEC, from about 0.7 to 0.3. Fig. 9c is the simulation diagram of flow velocity distribution curves of different n -value inks in the capillary. The results have shown that the smaller the value n of the ink represents, the smoother the flow velocity distribution along the nozzle diameter is. This will be more conducive to the extrusion owing to the reduction in the tendency of delamination. Therefore, the morphology of the ink during extrusion is more beneficial to the forming process.

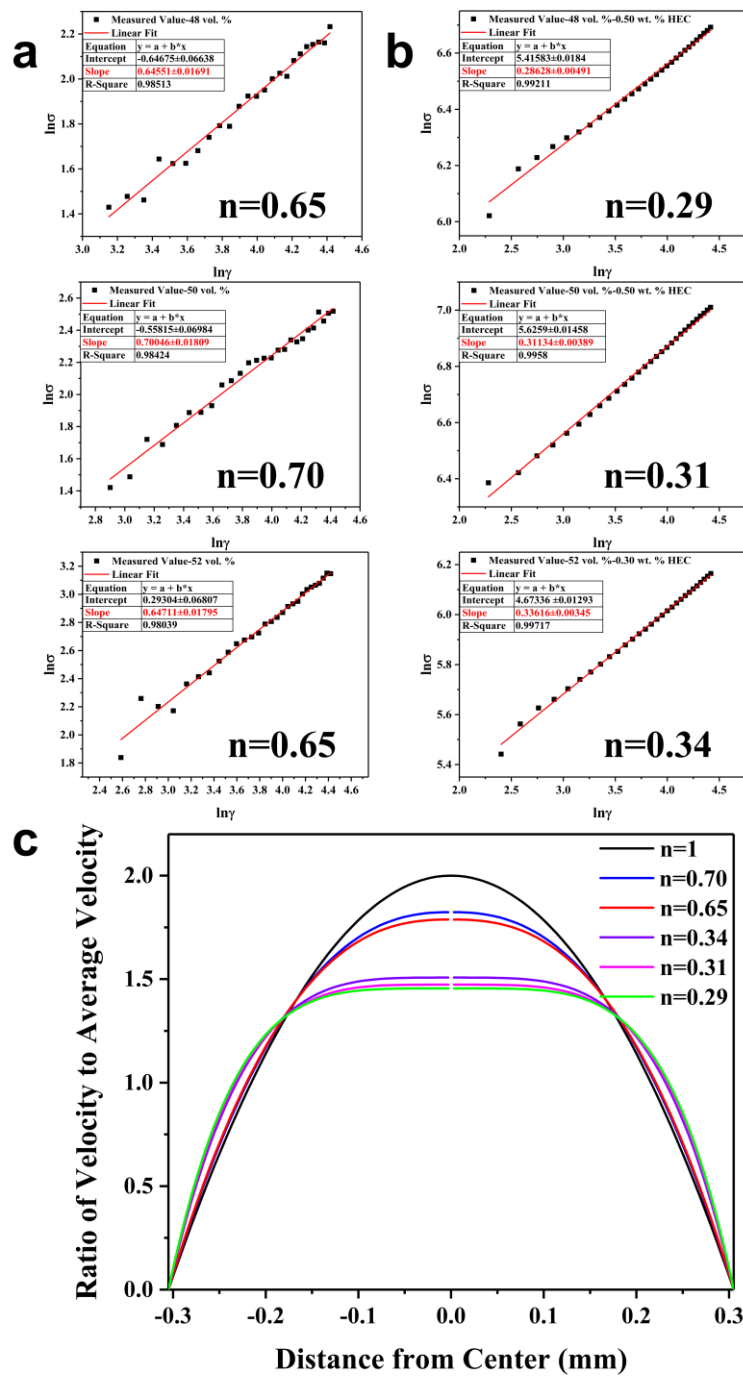


Fig. 9. (a) Non-Newtonian index of inks with different solids loading (without HEC). (b) Non-Newtonian index of inks with different solids loading (with different HEC). (c) Simulation diagram of flow velocity distribution in capillary.

3.6. Quantitative analysis of ink printability

Throughout the qualitative analysis of solid-liquid transition characteristics, structural recovery capacity, filament morphology and flow velocity distribution in Sections 3.1-3.5, the good printability of the inks including G4, G7, G8 and G11 have been demonstrated. In order to accurately and efficiently evaluate the printability of the ink from the rheological test results, the yield point, the flow point, the extrusion stress divided by the barrel radius, and the storage modulus of different inks have been summarized in Table 2. However, there is no obvious relationship between the composition of the ink and the yield points. Part of the reason is that G' in the amplitude sweep curve does not represent the obvious inflection point resulting in the error when selecting points. It has been observed that the value of the flow point should be more than 100 Pa to represent a good printable ink. Also, the storage modulus value under the static condition should be bounded between 2300 to 6000 Pa to maintain the sufficient shape retention and the extrusion stress should be in the range of 401 and 430 Pa for the appropriate extrusion pressure. As was expected, the stress in the extrusion test is quite different from the value of the flow point in the rotation test, where the specific rheological data by different rheological test methods cannot be validated against each other.

Table 2

Rheological test data of different component inks.

Ink ID	Yield Point τ_y [Pa]	Flow Point τ_f [Pa]	Storage Modulus G' [Pa]	Extrusion Stress E_p [Pa]
G1	-	-	-	-
G2	18	62	1000	229
G3	25	104	1700	296
G4	44	167	2300	401
G5	-	-	-	-
G6	20	57	2050	227
G7	22	105	3100	285
G8	38	175	3300	413
G9	-	-	-	-
G10	16	57	2100	257
G11	17	86	2400	304
G12	24	174	6000	229

It is worth noting that the above quantitative standards are applicable to aqueous ceramic slurries, but may not be applicable to, for example, hydrogel systems and organic solvent systems. However, it doesn't affect the applicability of this method for qualitative analysis of the ink printability. As there is neither a reliable definition to describe the plasticity nor a robust method to measure the plasticity in the field of ceramics, the plasticity is often called the extrudability, ductility, viscosity, consistency or printability. Moreover, due to the variety of rheological measurement methods and viscoelastic materials in this field, the rheological parameters have been unclearly provided and dependent of the inherent characteristics of the material such as the density, specific surface area, etc.

The experimental parameters for evaluating the printability of inks in this paper have been compared with the results of previous work as shown in Table 3. It can be seen that the criteria used to evaluate the printability of the ink in most existing researches is flow point and storage modulus. Basically, all references define the flow point of the inks with good printability in the range of 100 to 1000 Pa, while the definition of the storage modulus varies widely. The preparation of dense spanning structures requires inks with strong shape retention properties to resist gravity-induced deformation, so these inks exhibit extremely high storage modulus values. In contrast, for foam spanning structures as well as fully dense structures, the storage modulus values of the inks are lower due to low density or self-supporting of the structures. In addition, Peng et al. [31] believed that for different materials and different structures, the defined storage modulus value is also related to the specific weight of the ink, nozzle diameter, span length and layer height. Similarly, for fully dense structures, M' Barki et al. [13] defined a dimensionless parameter for evaluating the printability of the ink considering the density and surface tension of the ink, nozzle diameter and the height of the structure. In this work, the flow point, storage modulus and extrusion pressure have been used to quantitatively evaluate the printability of the ink. Also, the inks with good printability should exhibit shear thinning properties in the second stage of the O.R.O. test and not show liquid phase migration in the capillary extrusion test. The properties of the ink with good printability vary for different materials and target structures. How to formulate an effective and convenient way to evaluate the printability of ink is crucial to the development of direct ink writing. Future work could include using this method to evaluate the printability of inks for the preparation of other structures.

Table 3

Methodological comparisons.

Reference	Flow Point τ_f [Pa]	Storage Modulus G' [Pa]	Extrusion Stress E_p [Pa]	Structure Type
Zocca et al. [32]	$10^2 \sim 10^3$	$10^5 \sim 10^6$	-	All
Chan et al. [33]	>350	$2 \times 10^4 \sim 7 \times 10^5$	-	Dense spanning
Peng et al. [31]	>200	-	-	Dense spanning
Minas et al. [34]	>200	>2000	-	Foam spanning
Smay et al. [35]	~ 20	$\sim 10^5$	-	Dense spanning
Our approach	>100	$2300 \sim 6000$	$401 \sim 430$	Full dense

3.7. Printability of inks in DIW

It's universally acknowledged that the printability of the ink is ultimately determined by the morphology of the sample in DIW. Based on the tests and analyses in the previous sections, the G4, G7, G8 and G11 inks in Table 1 have been selected to represent the good printability verified by the predicted results. Fig. 10a has described the morphology of cubic samples written by different inks after extrusion. It has been observed that the structures of all samples are complete and no deformation. Special-shaped structures such as gear and pentagram box have been printed from G8 ink as shown in Fig. 10b. In addition, a fully dense pentagram block has been fabricated by combining the box printed from G8 ink with good shape retention and filled with G6 ink with better flowability. The predictions have been in good agreement with the experimental results, indicating the correctness and effectiveness of the

proposed approach.

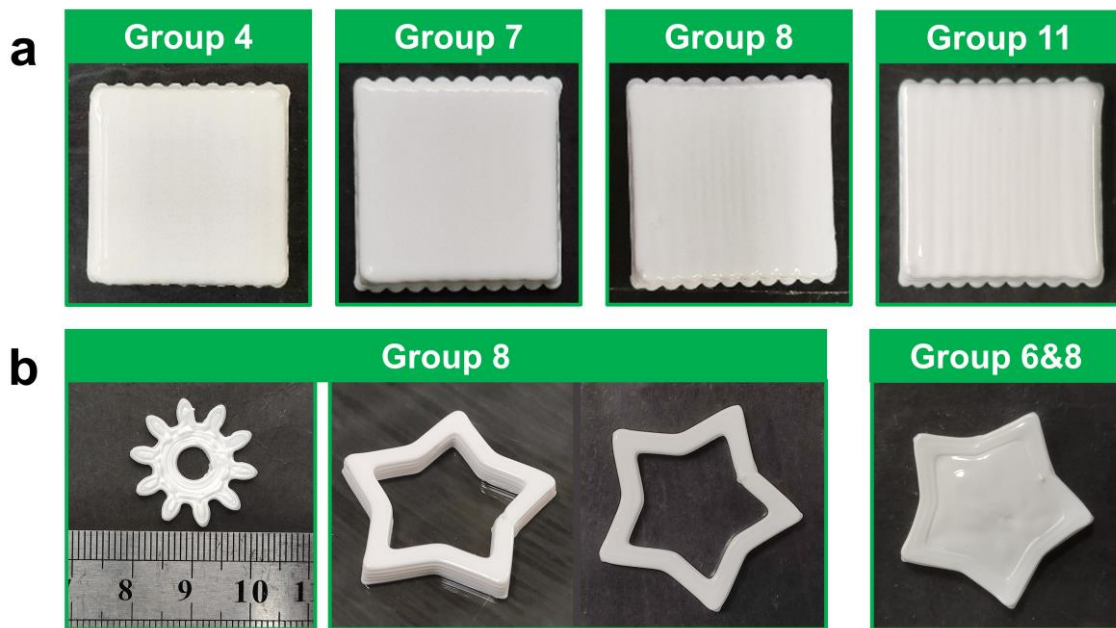


Fig. 10. Morphology of (a) cubic samples produced by different inks and (b) special-shaped samples: (left) gear, (center) pentagram box, (right) pentagram block.

Furthermore, the rheological properties of the doped Nd_2O_3 powder have been tailored in accordance to the results of previous sections for the preparation of the ink with good printability. The fabrication process of transparent Nd: YAG ceramics by DIW has been summarized in Fig. 11a, where includes the rheological test, printing, drying and polishing. The predicted printability of the ink using O.R.O. test is consistent with the experimental results as shown in Figs. 11b and 11c, where no visible printing defects in the sample have been identified. Also, the in-line transmittance of the polished sample has well agreed with the theoretical solution shown in Fig. 11d.

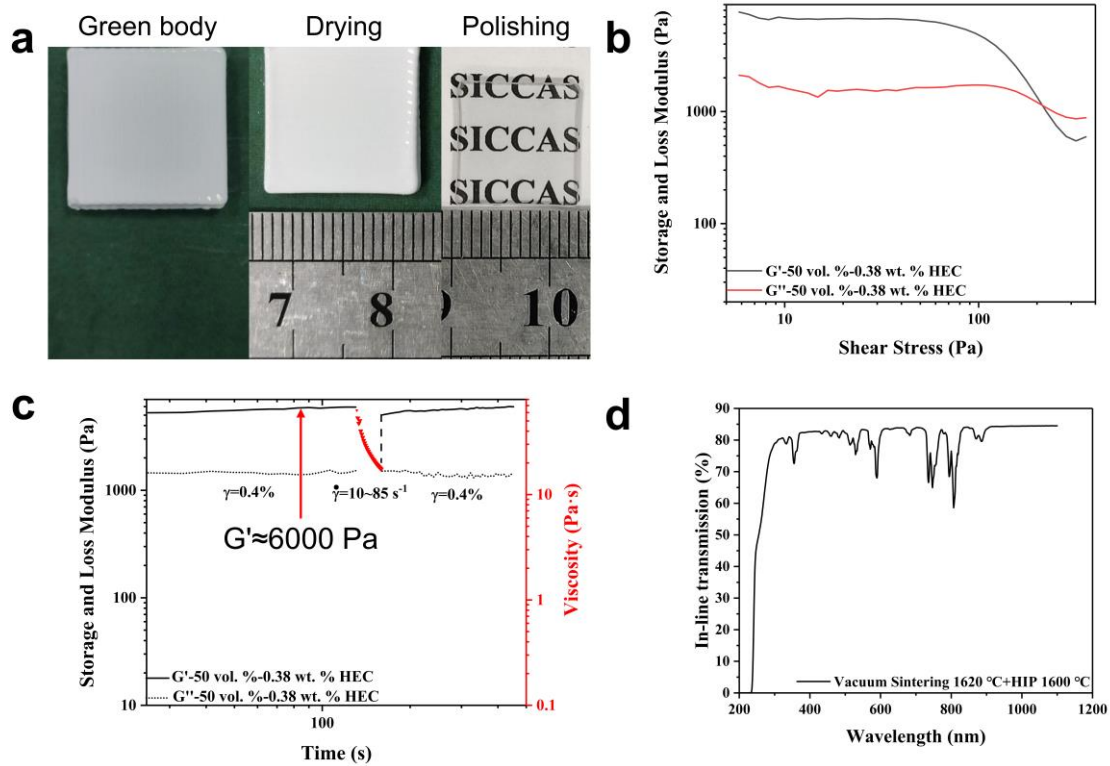


Fig. 11. (a) DIW process of fabricating transparent Nd:YAG ceramics. (b) Amplitude sweep curves. (c) O.R.O. curves. (d) In-line transmittance of the 1.8 mm thick polished 0.6 at. % Nd:YAG ceramic.

4. Conclusion

The printability of the water based ceramics slurry has been quantitatively evaluated by a novel experimental approach, which reflects on the combination of the developed O.R.O. test with capillary extrusion test for examining inks applicable to Direct Ink Writing (DIW). The amplitude sweep test and theoretical analysis and calculation have been applied to determine the low strain value (0.4%) within linear viscoelastic region in the oscillation stage and the high shear rate (85 s^{-1}) in the rotation stage of O.R.O. test, respectively. The integration of low-strain oscillation (L.S.O.) test with high-shear rotational (H.S.R.) test has enabled us to measure the changes in the rheological properties of the inks during the printing process. It is worth noting that the proposed experimental approach has taken full advantages of the

capillary extrusion test and the rotational rheometer whilst mitigating the side effect of pressure fluctuations on the stability of inks. Results have shown that the excellent qualities of printable inks have been quantitatively evaluated by two criteria, the storage modulus representing structural recovery capability and the extrusion stress indicating the flow characteristic of inks, with the values in the range of 2300-6000 Pa and 401-430 Pa, respectively. This has successfully provided a useful insight into the optimal printing process including adequate degassing and pre-pressing before printing. The flow velocity distribution of the inks along the nozzle diameter is closely related to the non-Newtonian index n , which drops drastically after adding HEC, from about 0.7 to 0.3. The results have shown that the smaller the value n of the ink represents, the smoother the flow velocity distribution along the nozzle diameter is. To further explore the superiority of the proposed approach over the traditional methods, alumina and yttria powders doped with neodymium oxide has been examined by its remarkable printability and the predicted rheological results have well agreed with the experimental data. Also, the in-line transmittance at 1064 nm for a 1.8 mm thick 0.6 at. % Nd: YAG ceramic can approach about 84.4% which is close to the theoretical value.. In conclusion, the proposed approach has the ability to quantitatively evaluate the printability of inks for DIW with high levels of accuracy and efficiency and also sheds a light on the possibility of a wider range of materials applicable to DIW and multi-phase additive manufacturing systems.

Acknowledgements

This work was supported by the National Key Research and Development Program of China (Grant No. 2017YFB0310500), the Scientific Instrument Developing Project of the Chinese Academy of Sciences (Grant No. YJKYYQ20180042) and National Natural Science Foundation of China (Grant No. 51875253).

Declaration of competing interest

The authors declare that they have no known competing financial interests or personal relationships that could have appeared to influence the work reported in this paper.

References

- [1] J.A. Lewis, Direct-write assembly of ceramics from colloidal inks, *Curr. Opin. Solid State Mater. Sci.* 6(3) (2002) 245-250.
- [2] J.A. Lewis, J.E. Smay, J. Stuecker, J. Cesarano III, Direct ink writing of three-dimensional ceramic structures, *J. Am. Ceram. Soc.* 89(12) (2006) 3599-3609.
- [3] Z. Seeley, T. Yee, N. Cherepy, A. Drobshoff, O. Herrera, R. Ryerson, S.A. Payne, 3D printed transparent ceramic YAG laser rods: Matching the core-clad refractive index, *Opt. Mater.* 107 (2020) 110121.
- [4] I.K. Jones, Z.M. Seeley, N.J. Cherepy, E.B. Duoss, S.A. Payne, Direct ink write fabrication of transparent ceramic gain media, *Opt. Mater.* 75 (2018) 19-25.
- [5] A.A. Wenbin Li, A. Martin, B. Kroehler, A. Henderson, T. Huang, J. Watts, G. Hilmas, M. Leu, Extrusion-based additive manufacturing of functionally graded ceramics, *J. Eur. Ceram. Soc.* 41(3) (2021) 2049-2057.
- [6] R. Dylla-Spears, T.D. Yee, K. Sasan, D. Nguyen, N.A. Dudukovic, J.M. Ortega, M.A. Johnson, O.D. Herrera, F.J. Ryerson, L.L. Wong, 3D printed gradient index glass optics, *Sci. Adv.* 6(47) (2020).
- [7] D. Nguyen, T.D. Yee, N.A. Dudukovic, K. Sasan, A.W. Jaycox, A.M. Golobic, E.B. Duoss, R. Dylla-Spears, 3D Printing of Compositional Gradients Using the Microfluidic Circuit Analogy, *Adv. Mater. Technol.* 4(12) (2019) 1900784.
- [8] J. S. Pelz, NicholasKu, W. T. Shoulders, M. A. Meyers, L. R. V. Gonzalez, Multi-material additive manufacturing of functionally graded carbide ceramics via active, in-line mixing, *Addit. Manuf.* 37 (2021) 101647.

-
- [9] H. Yuk, X.H. Zhao, A new 3D printing strategy by harnessing deformation, instability, and fracture of viscoelastic inks, *Adv. Mater.* 30(6) (2018) 1704028.
- [10] P. Forzatti, D. Ballardini, L. Sighicelli, Preparation and characterization of extruded monolithic ceramic catalysts, *Catal. Today.* 41(1-3) (1998) 87-94.
- [11] P. Forzatti, C. Orsenigo, D. Ballardini, F. Berti, On the relations between the rheology of TiO₂-based ceramic pastes and the morphological and mechanical properties of the extruded catalysts., *Prep. Catal. Vii.* 118 (1998) 787-796.
- [12] A. Corker, H.C.H. Ng, R.J. Poole, E. Garcia-Tunon, 3D printing with 2D colloids: designing rheology protocols to predict "printability" of soft-materials, *Soft Matter.* 15(6) (2019) 1444-1456.
- [13] A. M'Barki, L. Bocquet, A. Stevenson, Linking rheology and printability for dense and strong ceramics by direct ink writing, *Sci. Rep.* 7 (2017) 6017.
- [14] U. Yilmazer, D.M. Kalyon, Slip effects in capillary and parallel disk torsional flows of highly filled suspensions, *J. Rheol.* 33(8) (1989) 1197-1212.
- [15] M. Bayfield, J.A. Haggett, M.J. Williamson, D.I. Wilson, A. Zargar, Liquid phase migration in the extrusion of icing sugar pastes, *Food. Bioprod. Process.* 76(C1) (1998) 39-46.
- [16] J.M. Park, J.S. Han, C.W. Gal, J.W. Oh, K.H. Kate, S.V. Atre, Y. Kim, S.J. Park, Effect of binder composition on rheological behavior of PMN-PZT ceramic feedstock, *Powder. Technol.* 330 (2018) 19-26.
- [17] S. Majidi, G.H. Motlagh, B. Bahramian, B. Kaffashi, S.A. Nojoumi, I. Haririan, Rheological evaluation of wet masses for the preparation of pharmaceutical pellets by capillary and rotational rheometers, *Pharm. Dev. Technol.* 18(1) (2013) 112-120.
- [18] T. An, K.T. Hwang, J.H. Kim, J. Kim, Extrusion-based 3D direct ink writing of NiZn-ferrite structures with viscoelastic ceramic suspension, *Ceram. Int.* 46(5) (2020) 6469-6476.
- [19] X.P. Qin, G.H. Zhou, Y. Yang, J. Zhang, X. Shu, S.Z. Shimai, S.W. Wang, Gelcasting of transparent YAG ceramics by a new gelling system, *Ceram. Int.* 40(8) (2014) 12745-12750.
- [20] T.G. Mezger, *Applied Rheology*, Anton Paar GmbH, Austria, 2018.

-
- [21] Z.C. Chen, K. Ikeda, T. Murakami, T. Takeda, Effect of particle packing on extrusion behavior of pastes, *J. Mater. Sci.* 35(21) (2000) 5301-5307.
- [22] H.J. Liu, J. Liu, M.C. Leu, R. Landers, T.S. Huang, Factors influencing paste extrusion pressure and liquid content of extrudate in freeze-form extrusion fabrication, *Int J. Adv. Manuf. Technol.* 67(1-4) (2013) 899-906.
- [23] A. Perrot, C. Lanos, P. Estelle, Y. Meline, Ram extrusion force for a frictional plastic material: model prediction and application to cement paste, *Rheol. Acta.* 45(4) (2006) 457-467.
- [24] Q. Wu, J. Wu, *Polymer Rheology*, Higher Education Press, Beijing, 2014.
- [25] J. Travnickova, J. Havrda, F. Oujiri, The effect of particle-size on the rheological properties of ceramic paste, *Silikaty.* 33(1) (1989) 11-16.
- [26] E.B. Bagley, End corrections in the capillary flow of polyethylene, *J. Appl. Phys.* 28(5) (1957) 624-627.
- [27] B.R. R. Eisenschitz, K. Weissenberg, *Mitteil Deutsch, Materialspruefungsamt, Sonderheft.* 9(21) (1929).
- [28] J. Powell, S. Assabumrungrat, S. Blackburn, Design of ceramic paste formulations for co-extrusion, *Powder. Technol.* 245 (2013) 21-27.
- [29] J. Cai, A. Lv, J. Zhou, L Zang, *Cellulose Science and Materials*, Chemical Industry Press, Beijing, 2015.
- [30] M.J. Patel, J. Wedderburn, S. Blackburn, D.I. Wilson, Maldistribution of fluids in extrudates, *J. Eur. Ceram. Soc.* 29(5) (2009) 937-941.
- [31] E. Peng, D.W. Zhang, J. Ding, Ceramic robocasting: Recent achievements, potential, and future developments, *Adv. Mater.* 30 (2018) 1802404.
- [32] A. Zocca, P. Colombo, C.M. Gomes, J. Gunster, Additive manufacturing of ceramics: Issues, potentialities, and opportunities, *J. Am. Ceram. Soc.* 98(7) (2015) 1983-2001.
- [33] S.S.L. Chan, R.M. Pennings, L. Edwards, G.V. Franksa, 3D printing of clay for decorative architectural applications: Effect of solids volume fraction on rheology and

printability, *Addit. Manuf.* 35 (2020) 101335.

[34] C. Minas, D. Carnelli, E. Tervoort, A.R. Studart, 3D printing of emulsions and foams into hierarchical porous ceramics, *Adv. Mater.* 28 (2016) 9993–9999.

[35] J.E. Smay, J. Cesarano, J.A. Lewis, Colloidal inks for directed assembly of 3-D periodic structures, *Langmuir* 18(14) (2002) 5429–5437.